Unraveling the Edge Structures of Platinum(111)-Supported Ultrathin FeO Islands: The Influence of Oxidation State

Helene Zeuthen, Wilhelmine Kudernatsch, Lindsay R. Merte, Luis K. Ono, Lutz Lammich, Flemming Besenbacher, and Stefan Wendt*

Interdisciplinary Nanoscience Center (iNANO) and Department of Physics and Astronomy, Aarhus University, DK-8000 Aarhus C, Denmark

ABSTRACT We used high-resolution scanning tunneling microscopy to study the structure of ultrathin FeO islands grown on Pt(111). Our focus is particularly on the edges of the FeO islands that are important in heterogeneous catalysis, as they host the active sites on inversed catalysts. To imitate various reaction environments we studied pristine, oxidized, and reduced FeO islands. Oxidation of the FeO islands by O_2 exposure led to the formation of two types of O adatom dislocations and to a restructuring of the FeO islands, creating long O-rich edges and few short Fe-terminated edges. In contrast, reducing the FeO islands led to a dominance of Fe-rich edges and the occurrence of few and short O-rich edges. In addition, for reducing conditions we observed the formation of O vacancy dislocations on the FeO islands. Through the identification of O adatom and O vacancy dislocations known from closed ultrathin FeO films and geometrical considerations we unraveled the atomic structure of the predominant FeO boundaries of pristine, oxidized, and reduced FeO islands. The results indicate an astonishing flexibility of the FeO islands on Pt(111), since the predominant edge termination and the island shape depend strongly on the preparation conditions.

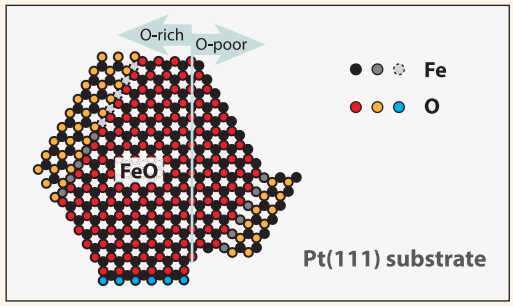

KEYWORDS: iron oxide · catalysis · model catalysts · edges · O adatom dislocations · O vacancy dislocations · scanning tunneling microscopy (STM)

Compounds of noble metals and transition metal oxides are widely used in heterogeneous catalysis.[1−6] In most cases the noble metals occur in the form of nanoparticles, while the oxides are used as support material. Traditionally, oxide supports have been considered catalytically inactive. However, more and more examples appear in the literature showing that oxide supports can interact with supported metal nanoparticles and affect catalytic reactions, particularly in the case of reducible transition metal oxides, such as titania and iron oxide.[6−13] The influence (both detrimental and promotional) of oxides in catalytic reactions can be particularly strong when the oxides cover the metal particles, forming so-called "inversed catalysts".[14−17] The most prominent example is the SMSI effect ("strong metal support interaction"), occurring when the noble metal−transition metal oxide compounds are heated in a reducing environment, such as H_2.[7,8,18] The SMSI effect has often been seen as a detrimental effect, as the covering oxide overlayer inhibits the adsorption of reactant molecules (encapsulation).[7,8,18,19]

There are, however, also cases where the formation of inversed catalysts leads to enhanced reactivity. An example was reported in 2010 by groups from Dalian and Hefei, who prepared monolayer (ML)-thin FeO islands on a Pt(111) substrate,[6,20,21] in the following denoted FeO_{is}/Pt(111). The FeO_{is}/Pt(111) model system is particularly interesting because the FeO−Pt(111) interface is accessible, exposing undercoordinated atoms at the cluster edges and rendering it catalytically very active.[20] Fu *et al.* denoted these sites as "coordinatively unsaturated ferrous (CUF) sites in close proximity to Pt",[20] whereas Gu *et al.*[22] and Sun *et al.*[23] in their density functional theory (DFT) studies described these sites as a "Pt−Fe cation ensemble".

* Address correspondence to swendt@phys.au.dk.

Received for review October 15, 2014 and accepted January 9, 2015.

Published online January 09, 2015
10.1021/nn505890v

Promising applications of FeO/Pt-based catalysts are the water-gas-shift (WGS) reaction[24] and the preferential oxidation of CO (PROX),[6,20,25] both of which are important for the production of pure H_2 with a minimal concentration of CO. For use in, for example, proton exchange membrane fuel cells[26] that are prone to deactivation due to CO poisoning, it is necessary to use very pure H_2 gas.[26,27] In both these applications, the benefit of FeO_{is}/Pt(111) over a conventional catalyst is the presence of dual adsorption sites.[6,20]

Despite the attention the FeO–Pt(111) interface has attracted, only little work has been focused on establishing the atomic structures of the edges of FeO islands. Existing models of the FeO islands and their edge structures have been deduced from the structure of the closed FeO ML film and exhibit only one or two different edge types, most of them Fe-terminated.[20−22,28−30] In their DFT modeling, Fu *et al.*[20] and Gu *et al.*[22] used an FeO ribbon consisting of three Fe columns and two O columns, which is Fe-terminated at the relevant, optimized edge, with the Fe atoms being 2-fold coordinated. Fu *et al.* assumed that the FeO islands are bordered by this single type of edge, which will be denoted as "Fe-edge" in the following. This simple model for the FeO boundaries was subsequently adopted by Xu *et al.*,[29] who combined X-ray photoelectron spectroscopy (XPS) and temperature-programed desorption (TPD) studies addressing the involvement of hydroxyls in the catalyzed CO oxidation reaction. In the experimental work by Yao *et al.*[21] a second edge type was introduced, which is suggested to be O-terminated. However, the focus by Yao *et al.* was more on finding the best conditions for the preparation of FeO_{is}/Pt(111) samples. Wang *et al.*[28] also proposed a second edge type, because these authors found an FeO island in scanning tunneling microscopy (STM) images characterized by edges of different length. Wang *et al.*[28] assigned the preferred, longer edges as Fe-edges, as originally suggested by Fu *et al.*, and the less frequent, shorter edges were suggested to also be Fe-terminated, but consisting of undercoordinated, one-fold coordinated Fe atoms instead of 2-fold coordinated Fe atoms. Generally, it has been assumed that all FeO islands consist of FeO in only one orientation relative to the Pt(111) surface, *i.e.*, the same orientation as the closed FeO ML film (see Figure 1).

Here we report on ultrathin, two-dimensional (2D) FeO islands grown on Pt(111) studied by high-resolution STM. We studied pristine, oxidized, and reduced FeO islands, which were observed in two different FeO orientations. Following oxidation of the FeO islands we distinguished two types of O adatom dislocations on the islands. At the same time, the FeO islands restructure, resulting in dominant O-rich edges with only a few, short Fe-terminated edges remaining. On the other hand, reducing the FeO islands led to structures dominated by Fe-rich edges and exhibiting very few and short O-terminated edges. In addition, we observed the formation of O vacancy dislocations on the FeO islands with some of them running parallel to the edges. On the basis of the identification of structures on the FeO islands such as O adatom and O vacancy dislocations it was possible to unravel the atomic structures of, in total, five different edge types at the FeO–Pt(111) interface.

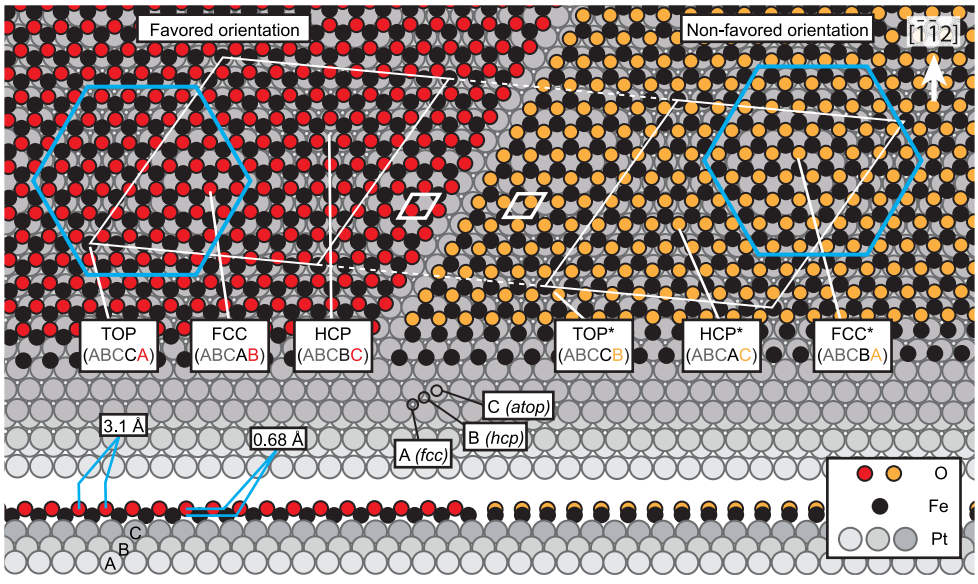

Figure 1. Top and side views of 2D FeO ML patches on Pt(111). The moiré-type superstructure unit cell (thin white lines) and the atomic unit cells (bold white lines) are indicated. Two FeO orientations are possible, distinguished by the placement of the O layer above the Fe layer. For the closed FeO ML film only the orientation on the left is observed experimentally (O atoms in red). O atoms in the nonfavored FeO film on the right are shown in yellow. This color-coding of the O atoms and the atomic unit cells is used throughout in the paper. The six different high-symmetry domains of the moiré superstructure are indicated. The hexagons (bold blue lines) illustrate how hexagonal FeO islands can be "cut" from FeO in both possible orientations.

RESULTS

Structure of the Closed Ultrathin FeO Film on Pt(111). We first review the well-established structure of closed FeO ML films grown on Pt(111) (see Figure 1), because this structure is the basis for understanding the edge structures of the FeO islands. In the experimentally observed structure of the closed FeO ML film, Fe and O form an incommensurate FeO overlayer on the Pt(111) substrate with a lattice spacing of ~3.1 Å, whereas the Pt(111) substrate is characterized by a lattice spacing of 2.77 Å. This closed FeO ML film is often denoted a "bilayer", since the FeO overlayer can be thought to be composed of an Fe layer in contact with Pt and an O layer away from it. With respect to the substrate, the FeO ML is rotated by ~0.6°, and the ~10% lattice mismatch between the two lattices leads to a moiré structure with a ~26 Å periodicity. The average rumpling (*i.e.*, the vertical distance between the Fe and O atoms) of the FeO film is ~0.68 Å, with the O atoms terminating the ultrathin film. The moiré structure exhibits three different high-symmetry domains [TOP, face-centered cubic (FCC), and hexagonal close-packed (HCP)] denoted according to the stacking order of the atoms in each domain. This atomic-scale structure of FeO/Pt(111) has been established by means of low-energy electron diffraction (LEED), STM, XPS, near-edge X-ray absorption fine structure (NEXAFS), and X-ray photoelectron diffraction (XPD) measurements.[31−36]

Also displayed in Figure 1 is a similar but energetically slightly unfavored structure of the FeO ML film.[37] This nonfavored FeO film on Pt(111) can be thought to be formed by rotating the film in favored FeO orientation by 60° or by shifting the O sublattice to adjacent Fe hollow sites. Considering the stacking order of the two topmost Pt layers, the nonfavored FeO film is not symmetrically equivalent to the film composed of FeO in favored orientation. Instead, the two FeO orientations are distinct, because the positions of the Pt atoms in the two topmost layers are different, as depicted by the stacking sequences in Figure 1. The three high-symmetry domains of the film consisting of FeO in nonfavored orientation are denoted TOP*, FCC*, and HCP*. For closed, stoichiometric FeO ML films, exclusively the favored FeO orientation is observed experimentally.[37,38] However, in case of islands on Pt(111) both FeO orientations occur, as will be shown below.

When, for example in the course of a surface reaction, FeO in favored orientation is transformed into FeO in nonfavored orientation, the TOP domains are turned into TOP* domains, the FCC domains into HCP* domains, and the HCP domains into FCC* domains (see Figure 1). This means that the TOP/TOP* domains are stationary upon FeO inversion and the FCC-type domains turn into HCP-type domains and HCP-type domains into FCC-type domains.[38] Accordingly, for FeO in favored and nonfavored orientations, the order of the high-symmetry domains along the long diagonal in the moiré unit cell is different. More specifically, in our presentation of the Pt(111) substrate in Figure 1, the order of the high-symmetry domains along the long diagonal in the moiré unit cell is TOP−FCC−HCP for FeO in favored orientation (from left to right), whereas for FeO in nonfavored orientation the order of the high-symmetry domains is TOP*−HCP*−FCC*.

The blue hexagons in Figure 1 illustrate how hexagonal FeO islands can be "cut out" from the FeO films of the two orientations. Assuming that highly undercoordinated O- and Fe-edge atoms do not occur, it can be recognized that hexagonal FeO islands are characterized by alternating O- and Fe-terminated edges. Moreover, it is clear that the island edges running along the same directions are terminated differently on the two FeO orientations. As for the closed FeO ML film, a hexagonal island consisting of favored FeO can be transformed into a "nonfavored" island by rotating it by 60°.

Pristine FeO Islands. We prepared "pristine" FeO islands by reactive deposition of Fe in an O_2 background (1×10^{-6} mbar) with the sample held at room temperature (RT). The coverage of FeO in all preparations was ~25% ML (where 1 ML = ?). Samples prepared in this way are denoted "*as-prepared* FeO_{is}/Pt(111)". Figure 2A shows a typical large-scale STM image acquired on an as-prepared FeO_{is}/Pt(111) sample that was flashed to 480 K. It can be seen that most FeO islands are of similar size and homogeneously distributed on the ~500 Å wide Pt terraces, the only exception being FeO islands along the Pt step edges on the lower terraces. The FeO islands obtained in this work resemble those previously described in the literature.[20,21,28]

The shape of the FeO islands can be described as irregular hexagons or truncated triangles. We found two main types of "truncated triangles", pointing either "up" or "down" at the given orientation of the substrate, corresponding approximately to the $[\bar{1}\bar{1}2]$ and $[11\bar{2}]$ directions on Pt(111). Analyzing the complete data set from which the STM images in Figure 2 were selected, we classified all 183 observed FeO islands as pointing either "up" or "down". In the example shown in Figure 2B, "down"-pointing FeO islands are indicated by white triangles, whereas "up"-pointing islands are indicated by blue triangles. We found that ~75% of the FeO islands were pointing "down" and ~25% pointing "up". As will be shown in the following, the predominant "down"-pointing FeO islands consist of FeO in the favored orientation, whereas "up"-pointing islands consist of FeO in the nonfavored orientation (see Figure 2C).

Figure 3 presents examples in which the orientation of the FeO in the islands could be revealed based on the observed order of the high-symmetry domains. The STM image in Figure 3A and the enlarged cut-outs

in Figure 3B,C were recorded on an as-prepared FeO_{is}/Pt(111) sample that was flashed to 480 K in 1×10^{-6} mbar O_2 and subsequently vacuum-annealed at 473 K for 4 min. Following this preparation, the FeO islands were more ordered and their shapes were closer to perfect triangles than obtained without the annealing step. Figure 3B and C depict interconnected FeO islands, presumably formed from two single islands during the preparation. In both examples the island on the left points "up" and the island on the right points "down". At the junction of the interconnected islands a bright line defect is visible in both examples. These line defects are identified as O adatom dislocation loops known from Pd(111)-supported FeO ML films.[39] Accordingly, the bright protrusions in the STM images at the junction originate from 4-fold O-coordinated Fe atoms.[39] Note that the formation of an O adatom dislocation is associated with inversion of the FeO at one side of the dislocation, which agrees with the finding that the two parts of the interconnected FeO islands point in opposite directions.

The STM image in Figure 3A was recorded in a known imaging mode ("mixed imaging mode #1"),[40] where the different domains can be distinguished by their apparent height and corrugation. In Figure 3B and C, the three high-symmetry domains are indicated by a square (FCC/FCC*), a triangle (HCP/HCP*), and a circle (TOP/TOP*), respectively. The order of the domains across the long moiré unit cell diagonal in the islands on the left is FCC–TOP–HCP (Figure 3B) and TOP–HCP–FCC (Figure 3C), respectively. Comparison with Figure 1 reveals that both these "up"-pointing islands are composed of FeO in nonfavored orientation. Analogously, we revealed that the "down"-pointing islands on the right in Figure 3B and C are composed of FeO in favored orientation. The schematic depicted in Figure 3D illustrates the structure of the FeO islands observed experimentally if the interconnected islands were perfect hexagons.

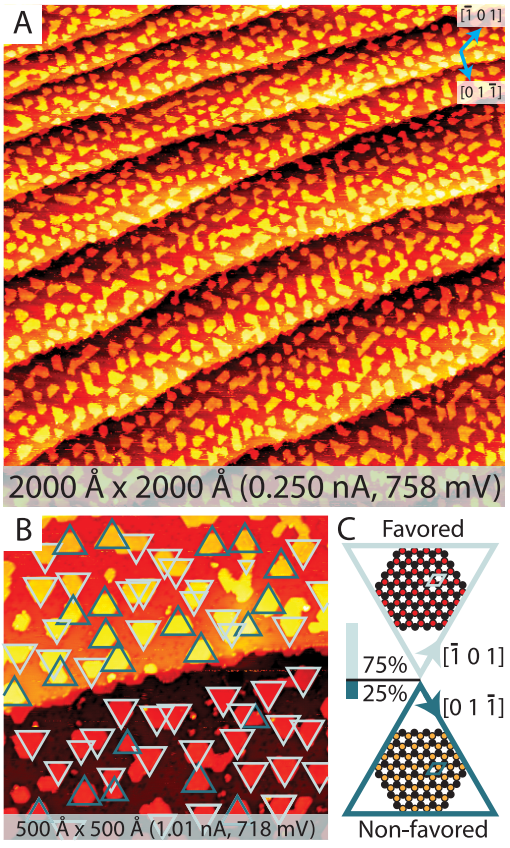

Figure 2. (A, B) STM images of pristine FeO islands acquired on as-prepared FeO_{is}/Pt(111) samples that were flashed to 480 K (A) and 466 K (B), respectively. (C) Schematic of the favored and nonfavored FeO orientations in hexagonal islands. In (B), superimposed, enclosing triangles highlight the O-edges. Arrows in (A) and (C) indicate the approximate directions on the Pt(111) substrate.

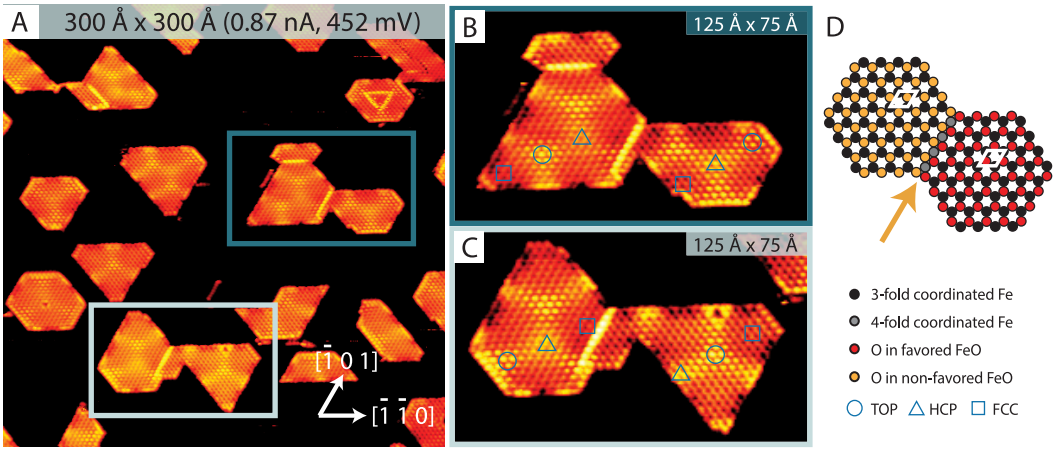

Figure 3. (A) STM image of pristine FeO islands, some of which are interconnected. Islands with O adatom dislocations are also imaged. An as-prepared FeO_{is}/Pt(111) sample was flashed to 480 K in 1.3×10^{-6} mbar O_2 and subsequently vacuum-annealed at 473 K for 4 min. Indicated areas in (A) are shown enlarged in (B) and (C), respectively. In (B) and (C), the high-symmetry domains are indicated. (D) Schematic of two interconnected hexagonal FeO islands, one composed of FeO in nonfavored orientation (left) and the other in favored orientation (right). Note the formation of an O adatom dislocation line at the interface (arrow). The atomic unit cells are indicated.

From the examples discussed in Figure 3 and further high-resolution STM images where the different domains on the FeO islands could be distinguished, we found that islands consisting of FeO in favored orientation always point "down", and islands consisting of FeO in nonfavored orientation always point "up". On this basis we conclude that an island's shape can be taken as a reliable indicator of the FeO orientation. Accordingly, even in cases where our STM images were not of the highest possible resolution it was possible to infer the FeO orientations based solely on the islands' shapes.

If the FeO orientation is known, it is also possible to assign the edges of the pristine FeO islands on well-ordered FeO_{is}/Pt(111) samples. With a look at the hexagons in Figures 1 and 3D as simplified models of the FeO islands, it becomes clear that the longer edges are O-terminated, whereas the shorter edges are Fe-terminated. This is valid for these interconnected FeO islands but also for most of the other FeO islands observed in Figure 3A. Accordingly, pristine FeO islands are characterized by the occurrence of both O-edges and Fe-edges. Under these preparation conditions the O-edges of these FeO islands are in most cases longer than the Fe-edges. This result, implying that "pristine" FeO islands exhibit a net excess of oxygen, is consistent with the occurrence of O adatom dislocation loops on some of the FeO islands and at the junctions between interconnected islands.

O-Rich FeO Islands. The STM image in Figure 4A was acquired on an as-prepared FeO_{is}/Pt(111) sample that was annealed at 475 K in 1.3×10^{-6} mbar O_2 for 2 min. The STM image shows a small FeO island with a bright, triangular line defect that is pointing "down". This triangular line defect resembles the known O adatom dislocation loops found on the closed FeO ML film grown on Pd(111),[39] which is structurally very similar to the FeO ML film grown on Pt(111). In addition, we observed O adatom dislocation loops on closed FeO ML films supported on Pt(111) appearing exactly like this,[41] thus further supporting that the triangular defect is indeed an O adatom dislocation loop. Figure 4B shows the suggested atomic structure of the FeO island. It can be seen that the Fe atoms along the O dislocation loop are 4-fold O-coordinated (gray Fe balls in Figure 4B), which explains their bright appearance in the STM images.[39]

A striking feature of the FeO island in Figure 4A is that three of its edges appear with bright contrast, which is comparable to the STM contrast characteristic for the triangular O adatom dislocations. This similar STM contrast and the oxidizing preparation conditions suggest that 4-fold O-coordinated Fe atoms occur also along these edges. Accordingly, we propose that the three edges with bright contrast are Fe-edges that have been oxidized, forming O-terminating edges. This interpretation is illustrated by the additional rows of O atoms in Figure 4B (depicted in yellow) along the edges that would be Fe-terminated on pristine FeO islands, resulting in 4-fold O-coordinated Fe atoms. Accordingly, we denote this type of edge as an "oxidized Fe-edge".

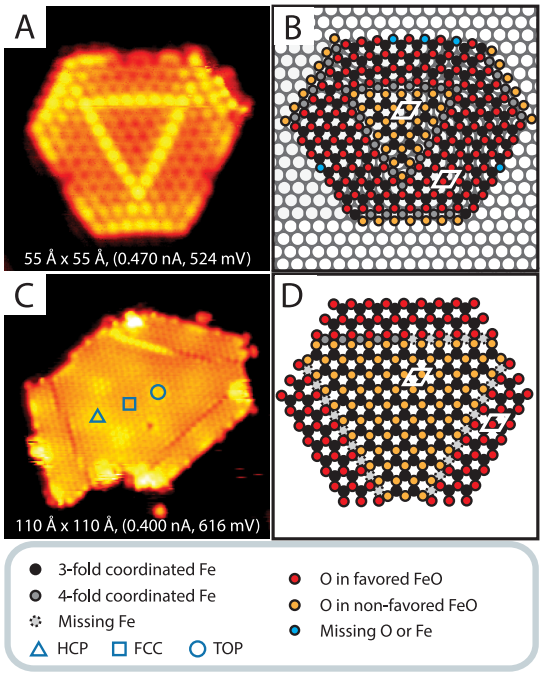

Figure 4. (A) STM image of an FeO island with a bright, triangular O adatom dislocation loop. This island is composed of FeO in favored orientation. An as-prepared FeO_{is}/Pt(111) sample was annealed in 1.3×10^{-6} mbar O_2 at 475 K for 2 min. (B) Atomic-scale model of the FeO island imaged in (A). (C) STM image of an island (FeO in nonfavored orientation) with dark and bright dislocations running parallel to the edges. In this case an as-prepared FeO_{is}/Pt(111) sample was exposed to 1.3×10^{-6} mbar O_2 at RT for 5 min. In (C), the high-symmetry domains are indicated. (D) Atomic-scale model of the inversion of the FeO island along the edges brought about by O dislocations. Note that the sketched island is only half the size of the FeO island depicted in (C).

The indentations appearing along the O edges of the FeO island depicted in Figure 4A could be caused by missing O atoms, represented by the blue disks in Figure 4B. Alternatively, the observed indentations might be explained by missing Fe atoms, since Fe atoms can diffuse relatively easily into the Pt substrate.[21,42] It is interesting to note that similar defects along the edges have been observed previously by Yao *et al.*[21] and Wang *et al.*[28]

Figure 4C presents a high-resolution STM image of another O-rich FeO island, acquired on an as-prepared FeO_{is}/Pt(111) sample that was exposed to 1.3×10^{-6} mbar O_2 for 5 min at RT. On this large, O-rich FeO island a moiré pattern can clearly be discerned. In addition, dark dislocation lines are recognized that run parallel to three of the island's edges. Note that dislocations of this kind have also been observed on closed FeO ML films on Pt(111).[41] Similar to the bright dislocations in Figure 4A, these dark dislocations are formed upon exposure to O_2, and they are running along the same

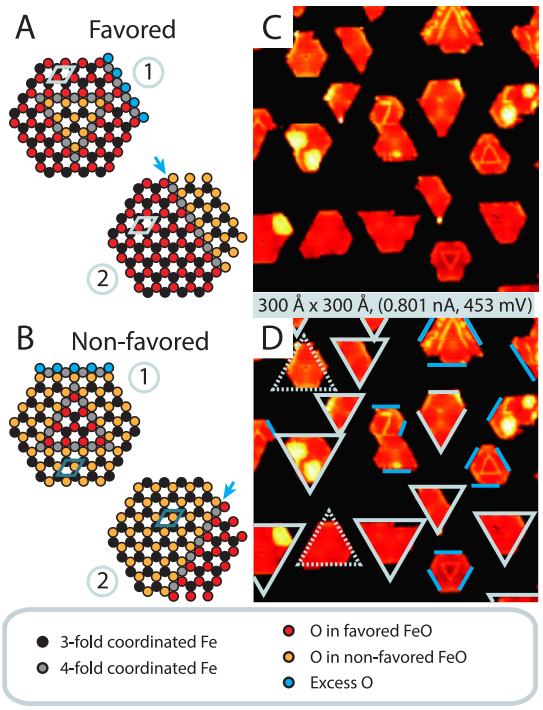

Figure 5. (A, B) Atomic-scale models for hexagonal FeO islands on Pt(111) with O-rich edges. Type (1) models are characterized by O adatom dislocation loops and oxidized Fe-edges. Type (2) models are characterized by O adatom dislocations along Fe-edges (blue arrows), transforming Fe-edges into O-edges. The atomic unit cells are indicated. (C) STM image of O-rich FeO islands. An as-prepared FeO_{is}/Pt(111) sample was annealed in 1.3×10^{-6} mbar O_2 at 475 K for 2 min. The white arrow indicates an O−Fe−O trilayer island. The image in (C) is duplicated in (D) for clarity. In (D), blue lines are drawn parallel to O adatom dislocations to indicate O-edges. White triangles mark O-edges of FeO islands with the FeO in favored (full lines) and nonfavored orientation (dashed lines), respectively.

directions as the bright dislocations. Because of the known imaging mode and the large size of this FeO island, it is possible to assign the three high-symmetry domains, as indicated in Figure 4C. The order of the domains, HCP−FCC−TOP (from left to right), indicates that the central part of this island consists of FeO in the nonfavored orientation.

The bright line defect at the top of Figure 4C looks very much like the triangular dislocation in Figure 4A, and, accordingly, we ascribe this line defect to an O adatom dislocation. The predominant, dark line defects on the same FeO island are also ascribed to O adatom dislocations; however, because of their dark appearance we believe that in these dislocations the Fe atoms are missing. Again, the appearance of the O adatom dislocations is connected with transformations of the edge types. In this case, Fe-edges were transformed into O-edges. The model sketched in Figure 4D is not a one-to-one model of the experimentally observed FeO island depicted in Figure 4C. Rather, an idealized, smaller FeO island is sketched, with O adatom dislocations running parallel to three of its edges. In these O adatom dislocations the Fe atoms (light gray balls) are missing. Within the three narrow FeO ribbons between the O adatom dislocations and the island edges, the O atoms (red balls) are shifted.

Figure 5A,B illustrate that the edges of triangular O adatom dislocation loops are running parallel to the original O-edges and that the corners of the O adatom dislocations point to the Fe-edges [favored FeO orientation, see Figure 5A(1); nonfavored FeO orientation, see Figure 5B(1)]. At the applied preparation conditions, the Fe-edges are mostly oxidized (blue balls). The two models marked (2) in Figures 5A,B illustrate that O adatom dislocation lines running parallel to Fe-edges invert the narrow FeO ribbons between the adatom lines and the edges. As a result, the (original) Fe-edges are transformed into O-edges.

On the basis of the geometrical considerations illustrated in Figure 5A,B we assign the edges of the islands in Figure 5C as follows (see Figure 5D): Blue lines running parallel to the O adatom dislocation loops correspond to O-edges, and the white triangles mark the O-edges of mostly triangular islands in favored (full lines) and nonfavored (dashed lines) FeO orientations. Thus, again we find that most of the edges are O-terminated. Many of the remaining edges appear bright and thus are most likely oxidized Fe-edges, as shown in blue in Figure 5A,B models (1). Only a few edges of the FeO islands in Figure 5C could not be assigned unambiguously; the others are clearly identified as O-terminated.

Finally, we note that upon extended exposure to O_2, some FeO islands also showed bright patches consisting of the O−Fe−O trilayer structure.[10,11,43] Examples of such patches are seen in the STM image in Figure 5C. However, O−Fe−O trilayer structures were mostly minor features at our preparation conditions, and, thus, they will not be discussed further.

We conclude from the STM data in Figures 4 and 5 that the O-rich FeO islands predominantly exhibit O edges. Specifically, the FeO islands depicted in Figure 4 are O-terminated along all their edges. This is caused by maintaining the original O-edges and either oxidizing the Fe-edges (Figure 4A,B) or inverting narrow FeO ribbons along the Fe-edges, thus transforming them into O-edges of inversely oriented FeO (Figure 4C,D).

O-Poor FeO Islands. Figure 6A shows a typical large-scale STM image acquired on an FeO_{is}/Pt(111) sample that was exposed to reducing conditions. More specifically, we started with an *as-prepared* FeO_{is}/Pt(111) sample that was exposed to CO at RT and finally vacuum-annealed at 580 K for 1 min (see Figure 6 for the precise preparation protocol). In Figure 6A, one part of the STM image (blue rectangle) is shown with different contrast to emphasize the presence of the O vacancy dislocations on the FeO islands. The O vacancy dislocations appear as dark lines, angles, and loops on the islands. Some of the present authors have previously studied O vacancy dislocations in great

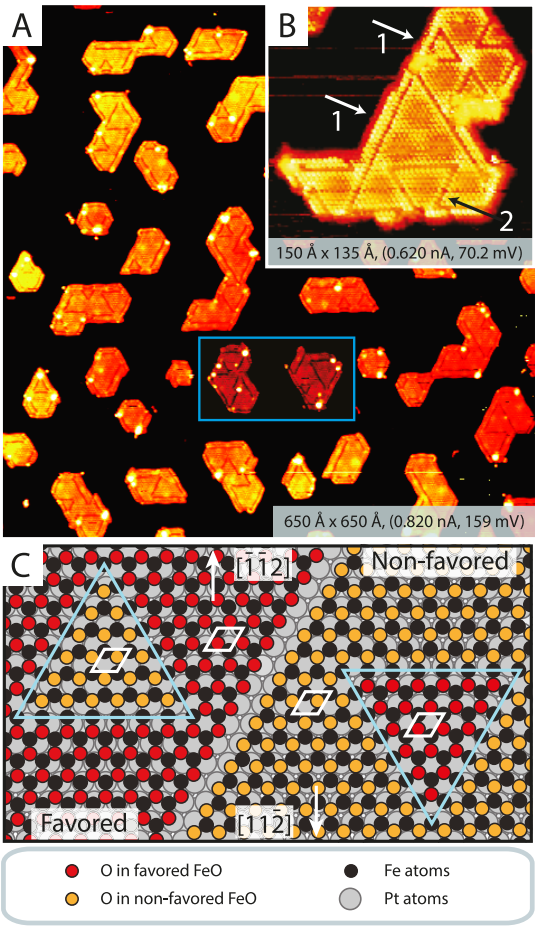

Figure 6. (A) STM image of O-poor FeO islands on Pt(111) with O vacancy dislocations. An as-prepared FeO_{is}/Pt(111) sample was annealed in 1.3×10^{-6} mbar O_2 at 475 K for 2 min, followed by 2 min exposure to CO at 1.3×10^{-7} mbar during scanning at RT and vacuum-annealing at 580 K for 1 min. A part of the STM image (indicated by the blue rectangle) is shown with different contrast to emphasize the presence of the O vacancy dislocations. (B) STM image acquired on an as-prepared FeO_{is}/Pt(111) sample that was exposed to 1.3×10^{-6} mbar O_2 at 476 K for 2 min, followed by exposure to 1.3×10^{-7} mbar H_2 at RT for 2 min and vacuum-annealing at 575 K for 1 min. (C) Ball models of O vacancy dislocation loops on islands with the FeO in favored (left) and nonfavored (right) orientations. O vacancy dislocation loops (large triangles) and the atomic unit cells are indicated.

detail on closed Pt(111)-supported FeO ML films that were reduced by atomic hydrogen.[37,38]

Following a very similar preparation, we acquired the high-resolution STM image depicted in Figure 6B. A quite large FeO island is imaged with several triangular O vacancy dislocations, most of which are pointing "up" (examples of triangular O vacancy dislocations are labeled 1). However, inside a large "up"-pointing dislocation loop a small triangular O vacancy dislocation is pointing "down" (labeled 2). This STM image was recorded in a tip-dependent imaging mode where the Fe atoms appear as protrusions.[40] From this and similar atomically resolved STM images recorded in known imaging modes we analyzed the registry of the FeO in and outside of the dislocations in a way described previously.[37] This analysis verified that the dislocations seen in Figure 6B are indeed O vacancy dislocations known from closed FeO ML films on Pt(111).

The orientation of the O vacancy dislocations provides information on the FeO orientation of the islands (see Figure 6C for an illustration). On the FeO patch in favored orientation on the left, the triangles are "up"-oriented with the apex pointing toward the [$\bar{1}\bar{1}$2] direction, whereas on the FeO area in nonfavored orientation on the right, the triangles are oriented "down" with the apex pointing toward the [11$\bar{2}$] direction. Accordingly, in the STM image depicted in Figure 6B, the dislocations indicated by arrows 1 are embedded in FeO in the favored orientation. Inside the O vacancy dislocations, the FeO is inverted. This inversion is confirmed by the enclosed, "down"-pointing triangular O vacancy dislocation (indicated by arrow 2).

Patches of FeO with inverted orientation were also frequently observed close to the edges of O-poor FeO islands. Examples for such inversions are presented in Figure 7. The high-resolution STM image depicted in Figure 7A shows an FeO island with several small triangular O vacancy dislocations with the apexes pointing "up". Accordingly, the large FeO island consists predominantly of FeO in the favored orientation. In addition to the small triangular O vacancy dislocations, the FeO island depicted in Figure 7A is characterized by long O vacancy dislocations running parallel to the edges, three of which are indicated by blue arrows. Because of these dislocations, the FeO within the ~10 Å wide ribbons between the edges and the line defects is inverted with respect to the FeO in the center part of this island. Thus, the (original) O-edges are converted to Fe-edges.

Another example of inversion of the FeO in proximity to the edges was observed on the FeO island depicted in Figure 7B. In this STM image a small, single, hexagonal FeO island (favored FeO orientation) is seen with O vacancy dislocations along three of its edges. The model in Figure 7C illustrates the proposed atomic-scale structure of the small FeO island. Along the original O-edges, O vacancy dislocation lines have formed *via* the removal of O rows and the shifting of a narrow ribbon of O atoms along the edges (O atoms in yellow). Thus, the O-edges are inverted into Fe-edges. As a consequence, all the edges of the FeO island are Fe-terminated.

The bright, round protrusions at the edge of the FeO island depicted in Figure 7B are omitted in our ball model of the atomic-scale structure. These protrusions at the ends of the inverted FeO ribbons might originate from reconstructions or adsorbates, *e.g.*, water or another species from the residual gas. As depicted in the model (Figure 7C), the areas where two inverted FeO ribbons meet are characterized by highly undercoordinated Fe atoms. It can be envisaged that these configurations shown in our model do not exist

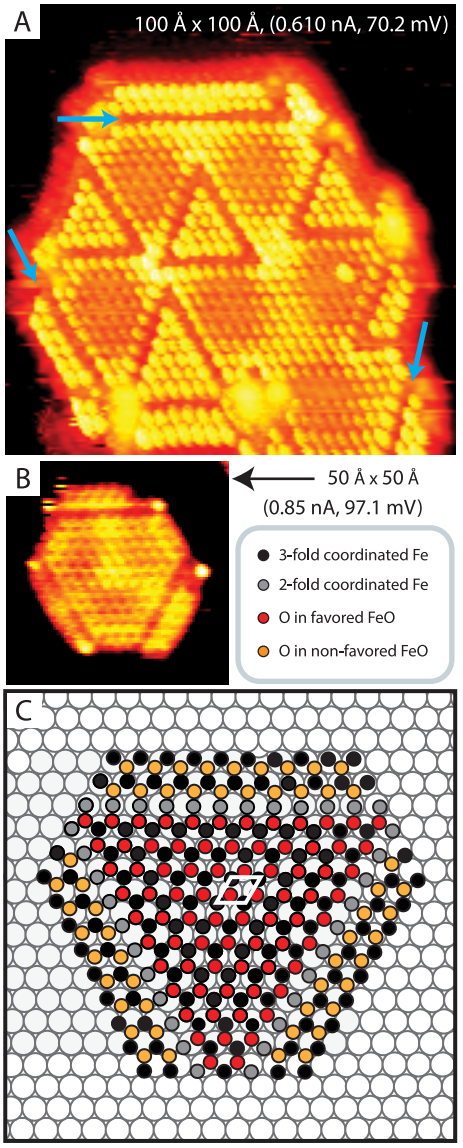

Figure 7. (A, B) STM images of O-poor FeO islands on Pt(111) with O vacancy dislocations, both of which are composed of FeO in the favored orientation. In (A), an as-prepared FeO_{is}/Pt(111) sample was 2 min annealed in 1.3 × 10^{-6} mbar O_2 at 475 K, followed by 2 min H_2 exposure at RT (1.3 × 10^{-7} mbar) and subsequently vacuum-annealed at 575 K for 1 min. The STM image in (B) was acquired on an as-prepared FeO_{is}/Pt(111) sample that was flashed to 475 K in 1.3 × 10^{-6} mbar O_2 and subsequently vacuum-annealed at 475 K for 2 min. (C) Schematic of an FeO island with O vacancy dislocations along O-edges. The O vacancy dislocations along O-edges invert the FeO, transforming the O-edges into Fe-edges.

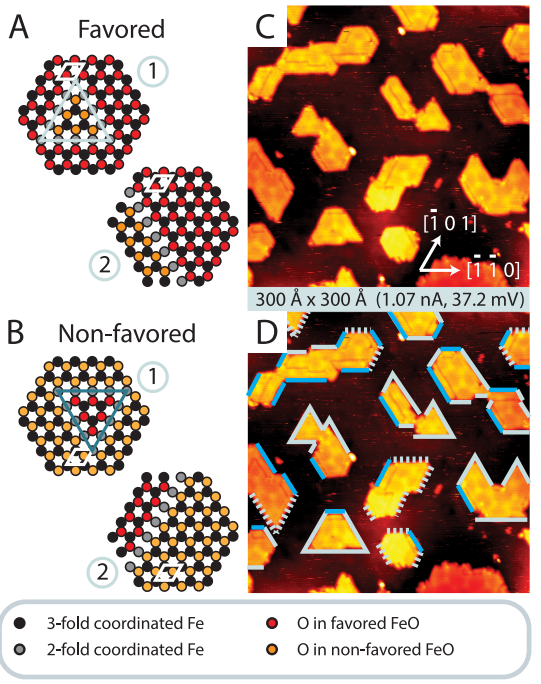

Figure 8. (A, B) Models of hexagonal O-poor FeO islands on Pt(111). Type (1) models are characterized by O vacancy dislocation loops, and type (2) models are characterized by O vacancy dislocations along O-edges, transforming them into Fe-edges. (C) STM image acquired on an as-prepared FeO_{is}/Pt(111) sample that was flashed to 475 K in 1.3 × 10^{-6} mbar O_2 and subsequently vacuum-annealed at 457 K for 2 min. The image in (C) is duplicated in (D) for clarity. Lines in (D) mark different types of Fe-terminated edges. Blue lines mark O-edges transformed into Fe-edges by a nearby parallel dislocation, and white lines mark pristine Fe-edges in the favored orientation (full lines) and nonfavored orientations (dashed lines), respectively.

experimentally, because they are probably not stable, leading to an unknown reconstruction or clustering of residual material.

As was the case for the O-rich islands, geometric considerations are helpful for unraveling the edge type of O-poor FeO islands. In Figure 8A,B, hexagonal islands labeled 1 exhibit triangular O vacancy dislocation loops, and the edges of these O dislocations are running parallel to the Fe-edges. The islands labeled 2 show O vacancy dislocation lines that are running parallel to one of the edges (original O-edges). The O atoms in the narrow ribbons of FeO between the O vacancy dislocation and the edges are shifted inward to adjacent hollow sites. In this way the (original) O-edges are transformed into Fe-edges. Hexagonal FeO islands are characterized by alternating Fe- and O-edges (as seen for the islands labeled 1 in Figure 8A,B and in Figure 2C), whereas perfectly triangular FeO islands are characterized by the occurrence of only one edge type. O-Deficient triangular FeO islands are bounded solely by Fe-edges (see Figure 2C). Accordingly, such islands with the FeO in favored and nonfavored orientations point in opposite directions. Specifically, triangularly shaped, Fe-terminated FeO islands are characterized by apexes pointing "down" and "up" for FeO in favored and nonfavored orientations, respectively.

Next, we describe the edge structures of the O-deficient FeO islands observed in Figure 8C. This STM image was acquired on an as-prepared FeO_{is}/Pt(111) sample that was first flashed to 475 K in O_2 and subsequently vacuum-annealed for 2 min at 457 K. The FeO islands observed after vacuum-annealing are more elongated than their nonannealed counterparts.

The elongation occurs along the directions of the Fe-edges ([$\bar{1}$10], [$\bar{1}$01], and [01$\bar{1}$] for islands consisting of FeO in favored orientation) and allows the FeO islands to terminate with more Fe-edges, and thus fewer O-edges. Furthermore, many of the islands exhibit long O vacancy dislocation lines running parallel to their edges. In Figure 8D, the STM image shown in Figure 8C is duplicated, and the assignments of the edges are indicated. Blue lines mark edges with a parallel O vacancy dislocation in proximity. These edges are assigned as O-edges that have been transformed into Fe-edges by the nearby O vacancy dislocation. Triangular islands are assumed to be Fe-terminated at the applied preparation conditions, and the Fe-edges on the islands consisting of favored and nonfavored FeO are marked by full and dashed bright lines, respectively. It can be seen that Fe-edges, either the original ones or transformed ones running parallel to O vacancy dislocations (original O edges), are preferred at O-deficient conditions.

We conclude from the STM data in Figures 6, 7, and 8 that O-poor FeO islands are characterized by predominant Fe-terminated edges. Original O-edges are inverted to Fe-edges by the formation of O vacancy dislocations. Both the formation of triangular O vacancy dislocations on the FeO islands and O vacancy dislocation lines running parallel to original O-edges were observed. The orientation of triangular O vacancy dislocations indicates whether the FeO occurs in favored or nonfavored orientation.

DISCUSSION

Above we have shown that Pt(111)-supported ultrathin, 2D FeO islands occur in both possible orientations of FeO, which are distinct by the placement of the O layer above the Fe layer. This contrasts the situation found for stoichiometric, closed FeO ML films on Pt(111), where exclusively the favored FeO orientation is observed experimentally. We propose that this difference is related to the fact that the two FeO orientations are energetically almost degenerate. Upon reactive Fe deposition, islands grow simultaneously composed of FeO in both orientations, since the FeO orientation is initially defined by the nucleation sites at which the island growth starts. Both FeO orientations outlast the completion of the FeO_{is}/Pt(111) preparation, because no or few interactions occur between individual FeO islands at this low coverage. The situation is different for closed FeO ML films, where FeO patches grown from different nucleation sites on the substrate, characterized by different FeO orientations, will inevitably interact with each other (because of the higher FeO coverage), finally leading to the occurrence of only one FeO orientation. Of course, this will be the energetically slightly favored FeO orientation.

Because of the strong interaction between the FeO overlayer and the Pt(111) substrate,[20,44] the FeO–Pt(111) interface has previously been considered as rather firm. In other words, the suggested "interface confinement effect"[6,20] has led to the assumption that FeO boundaries, and with this the proposed active CUF sites, would be very stable.[20] In addition, only few edge types have been considered at the FeO–Pt(111) interface,[20–22,28–30] as outlined in the introduction. However, the presented high-resolution STM data show that this view is incomplete. First, a rich variety of edge structures exist depending on the preparation conditions, as summarized in Figure 9. In addition to simple Fe- and O-edges we identified "oxidized Fe-edges". Second, it appears that the FeO–Pt(111) interface is quite dynamic, meaning that the FeO edges cannot be considered as static, very stable sites as anticipated previously. For example, the Fe-edges can be transformed into O-edges and *vice versa via* FeO inversion within narrow FeO ribbons running parallel to the edges. The astonishing flexibility of the 2D FeO islands on Pt(111), depending on the applied preparation conditions, is based on several points: (1) two possible FeO orientations exist for the FeO islands, (2) O vacancy and O adatom dislocations can be formed rather easily, and (3) the changes occurring at the edges and on the FeO islands are interconnected. These interesting phenomena can be understood essentially by considering that each single FeO island interacts "individually" with its environment and that some of the constraints existing in closed FeO ML films are absent.

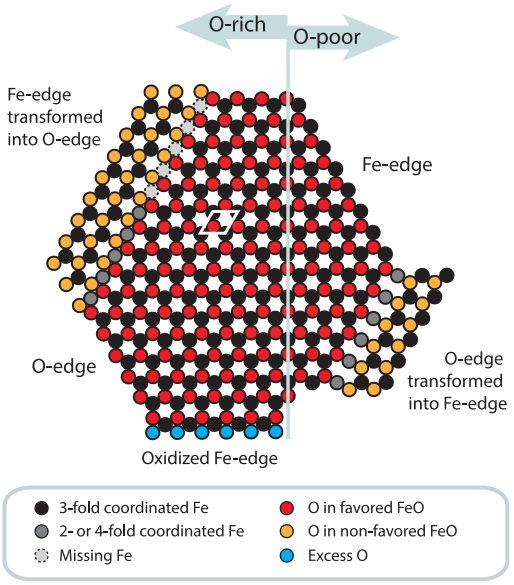

Figure 9. (A, B) Summary of the identified structural features on ultrathin 2D FeO islands on Pt(111). In addition to the various edge-types, two types of O adatom dislocations and one type of O vacancy dislocation lines were identified.

CONCLUSIONS

We have studied ultrathin FeO islands grown on Pt(111) by high-resolution STM. Surprisingly, we found that the FeO islands occur in two different FeO orientations, in contrast to what is known for closed FeO ML

films. The ratio between islands with FeO in favored and nonfavored orientation is ~3:1. Furthermore, we revealed the detailed atomic structure of five different edge types, two of which are characteristic for pristine FeO islands. Following their initial preparation, the pristine FeO islands were either oxidized by exposing them to O_2 or reduced using various methods including vacuum-annealing. Oxidation of the FeO islands resulted in substantial changes. For example, two types of O adatom dislocations were formed: one appearing bright that is analogous to the O adatom dislocations observed on FeO/Pd(111) and another, new type that appears dark in the STM images. In addition, the boundaries changed upon oxidation: Fe-edges were oxidized or transformed into O-edges by formation of O adatom dislocations, and the shape of the FeO islands changed, exposing fewer of the Fe-terminated edges. Reducing the islands led to different shapes of the FeO islands, exposing fewer O-rich edges. Furthermore, O vacancy dislocations similar to those found on the closed FeO ML film grown on Pt(111) formed on the FeO islands and along the edges. On the basis of the known structures of both O adatom and O vacancy dislocations, we deduced the atomic structures of the predominant FeO boundaries. The knowledge of these edge structures is not only interesting for fundamental research but very crucial in catalysis, as they host the active sites.[5,11]

METHODS

The STM experiments were conducted in a UHV chamber with a base pressure of 1×10^{-10} mbar equipped with a home-built Aarhus STM,[45,46] an electron-beam evaporator (Oxford Applied Research, EGCO4), and standard facilities for sample preparation and characterization. The Pt(111) sample was cleaned by cycles of Ar^+-sputtering and subsequent vacuum-annealing up to ~1100 K. If necessary, the sample was annealed in 5×10^{-8} mbar O_2 at 850 K to oxidize any carbon species on the surface. FeO islands covering ~25% of the surface were grown by reactive deposition of Fe (Goodfellow, 99.99%) in a background of 1×10^{-6} mbar O_2 with the sample held at RT ("as-prepared FeO_{is}/Pt(111)"). Subsequently, the samples were flash-annealed to achieve the wanted size of the FeO islands and to remove excess O from the Pt(111) substrate. Gas exposures were accomplished by backfilling the chamber and determined from the background pressures and the exposure times.

Oxidation of pristine FeO islands was achieved by backfilling the UHV chamber with O_2. During the O_2 exposures, the sample was either held at RT or annealed at temperatures between 400 and 500 K. Contrary to what is known for closed FeO ML films, neither atomic oxygen[39,41] nor high O_2 pressures[10,11,43] were required to oxidize the FeO islands. Reduction of as-prepared FeO_{is}/Pt(111) samples was achieved either solely by vacuum-annealing or by H_2 or CO exposure, followed by vacuum-annealing. Annealing in UHV was conducted at temperatures up to 580 K, similarly to that by Yao *et al.*[21]

Throughout, the samples were imaged in constant current mode and STM imaging was conducted at RT. A mechanically cut Pt/Ir tip was used. STM images were acquired in different, known imaging modes, which could be recognized based on our previous work.[40] Typically, scanning parameters were chosen in the range 0.25−1.1 nA and 40−800 mV.

Conflict of Interest: The authors declare no competing financial interest.

Acknowledgment. We acknowledge the support of this work by the Villum Kahn Rasmussen Foundation, the Carlsberg Foundation, and the European Research Council through an Advanced ERC grant (F.B.).

REFERENCES AND NOTES

1. Campbell, C. T. Ultrathin Metal Films and Particles on Oxide Surfaces: Structural, Electronic and Chemisorptive Properties. *Surf. Sci. Rep.* **1997**, *27*, 1–111.
2. Gandhi, H. S.; Graham, G. W.; McCabe, R. W. Automotive Exhaust Catalysis. *J. Catal.* **2003**, *216*, 433–442.
3. Haruta, M. Gold as a Novel Catalyst in the 21st Century: Preparation, Working Mechanism and Applications. *Gold Bull.* **2004**, *37*, 27–36.
4. Chen, M. S.; Cal, Y.; Yan, Z.; Gath, K. K.; Axnanda, S.; Goodman, D. W. Highly Active Surfaces for CO Oxidation on Rh, Pd, and Pt. *Surf. Sci.* **2007**, *601*, 5326–5331.
5. Cuenya, B. R. Synthesis and Catalytic Properties of Metal Nanoparticles: Size, Shape, Support, Composition, and Oxidation State Effects. *Thin Solid Films* **2010**, *518*, 3127–3150.
6. Fu, Q.; Yang, F.; Bao, X. H. Interface-Confined Oxide Nanostructures for Catalytic Oxidation Reactions. *Acc. Chem. Res.* **2013**, *46*, 1692–1701.
7. Tauster, S. J.; Fung, S. C.; Garten, R. L. Strong Metal-Support Interactions - Group-8 Noble-Metals Supported on TiO_2. *J. Am. Chem. Soc.* **1978**, *100*, 170–175.
8. Tauster, S. J. Strong Metal-Support Interactions. *Acc. Chem. Res.* **1987**, *20*, 389–394.
9. Goodman, D. W. "Catalytically Active Au on Titania": Yet Another Example of a Strong Metal Support Interaction (SMSI)? *Catal. Lett.* **2005**, *99*, 1–4.
10. Sun, Y. N.; Qin, Z. H.; Lewandowski, M.; Carrasco, E.; Sterrer, M.; Shaikhutdinov, S.; Freund, H. J. Monolayer Iron Oxide Film on Platinum Promotes Low Temperature CO oxidation. *J. Catal.* **2009**, *266*, 359–368.
11. Lewandowski, M.; Sun, Y. N.; Qin, Z. H.; Shaikhutdinov, S.; Freund, H. J. Promotional Effect of Metal Encapsulation on Reactivity of Iron Oxide Supported Pt Catalysts. *Appl. Catal. A: Gen.* **2011**, *391*, 407–410.
12. Green, I. X.; Tang, W. J.; Neurock, M.; Yates, J. T., Jr. Spectroscopic Observation of Dual Catalytic Sites during Oxidation of CO on a Au/TiO_2 Catalyst. *Science* **2011**, *333*, 736–739.
13. Willinger, M. G.; Zhang, W.; Bondarchuk, O.; Shaikhutdinov, S.; Freund, H. J.; Schlögl, R. A Case of Strong Metal-Support Interactions: Combining Advanced Microscopy and Model Systems to Elucidate the Atomic Structure of Interfaces. *Angew. Chem., Int. Ed.* **2014**, *53*, 5998–6001.
14. Schoiswohl, J.; Sock, M.; Chen, Q.; Thornton, G.; Kresse, G.; Ramsey, M. G.; Surnev, S.; Netzer, F. P. Metal Supported Oxide Nanostructures: Model Systems for Advanced Catalysis. *Top. Catal.* **2007**, *46*, 137–149.
15. Surnev, S.; Fortunelli, A.; Netzer, A.; P, F. Structure−Property Relationship and Chemical Aspects of Oxide−Metal Hybrid Nanostructures. *Chem. Rev.* **2013**, *113*, 4314–4372.
16. Rodriguez, J. A.; Hrbek, J. Inverse Oxide/Metal Catalysts: A Versatile Approach for ActivityTests and Mechanistic Studies. *Surf. Sci.* **2010**, *604*, 241–244.
17. Rodriguez, J. A.; Ma, S.; Liu, P.; Hrbek, J.; Evans, J.; Perez, M. Activity of CeO_x and TiO_x Nanoparticles Grown on Au(111) in the Water-Gas Shift Reaction. *Science* **2007**, *318*, 1757–1760.
18. Haller, G. L.; Resasco, D. E. Metal Support Interaction - Group-VIII Metals and Reducible Oxides. *Adv. Catal.* **1989**, *36*, 173–235.

19. Bonanni, S. B. S.; Ait-Mansour, K.; Brune, H.; Harbich, W. Overcoming the Strong Metal-Support Interaction State: CO Oxidation on TiO_2(110)-Supported Pt Nanoclusters. *ACS Catal.* **2011**, *1*, 385–389.
20. Fu, Q.; Li, W.-X.; Yao, Y.; Liu, H.; Su, H.-Y.; Ma, D.; Gu, X.-K.; Chen, L.; Wang, Z.; Zhang, H.; Wang, B.; Bao, X. Interface-Confined Ferrous Centers for Catalytic Oxidation. *Science* **2010**, *328*, 1141–1144.
21. Yao, Y. X.; Fu, Q. A.; Wang, Z.; Tan, D. L.; Bao, X. H. Growth and Characterization of Two-Dimensional FeO Nano-islands Supported on Pt(111). *J. Phys. Chem. C* **2010**, *114*, 17069–17079.
22. Gu, X. K.; Ouyang, R. H.; Sun, D. P.; Su, H. Y.; Li, W. X. CO Oxidation at the Perimeters of an FeO/Pt(111) Interface and How Water Promotes the Activity: A First-Principles Study. *ChemSusChem* **2012**, *5*, 871–878.
23. Sun, D. P.; Gu, X. K.; Ouyang, R. H.; Su, H. Y.; Fu, Q.; Bao, X. H.; Li, W. X. Theoretical Study of the Role of a Metal-Cation Ensemble at the Oxide-Metal Boundary on CO Oxidation. *J. Phys. Chem. C* **2012**, *116*, 7491–7498.
24. Ratnasamy, C.; Wagner, J. P. Water Gas Shift Catalysis. *Catal. Rev.* **2009**, *51*, 325–440.
25. Park, E. D.; Lee, D.; Lee, H. C. Recent Progress in Selective CO Removal in a H_2-Rich Stream. *Catal. Today* **2009**, *139*, 280–290.
26. Mehta, V.; Cooper, J. S. Review and Analysis of PEM Fuel Cell Design and Manufacturing. *J. Power Sources* **2003**, *114*, 32–53.
27. Acres, G. J. K.; Frost, J. C.; Hards, G. A.; Potter, R. J.; Ralph, T. R.; Thompsett, D.; Burstein, G. T.; Hutchings, G. J. Electrocatalysts for Fuel Cells. *Catal. Today* **1997**, *38*, 393–400.
28. Wang, W.; Zhang, H.; Wang, W. H.; Zhao, A. D.; Wang, B.; Hou, J. G. Observation of Water Dissociation on Nanometer-Sized FeO Islands Grown on Pt(111). *Chem. Phys. Lett.* **2010**, *500*, 76–81.
29. Xu, L. S.; Wu, Z. F.; Zhang, Y. L.; Chen, B. H.; Jiang, Z. Q.; Ma, Y. S.; Huang, W. X. Hydroxyls-Involved Interfacial CO Oxidation Catalyzed by FeO_x(111) Monolayer Islands Supported on Pt(111) and the Unique Role of Oxygen Vacancy. *J. Phys. Chem. C* **2011**, *115*, 14290–14299.
30. Wang, Y.; Zhang, H. M.; Yao, X. D.; Zhao, H. J. Edges of FeO/Pt(111) Interface: A First-Principle Theoretical Study. *J. Phys. Chem. C* **2013**, *117*, 1672–1676.
31. Vurens, G. H.; Maurice, V.; Salmeron, M.; Somorjai, G. A. Growth, Structure and Chemical-Properties of FeO Overlayers on Pt(100) and Pt(111). *Surf. Sci.* **1992**, *268*, 170–178.
32. Galloway, H. C.; Benitez, J. J.; Salmeron, M. Growth of FeO_x on Pt(111) Studied by Scanning-Tunneling-Microscopy. *J. Vac. Sci. Technol. A* **1994**, *12*, 2302–2307.
33. Schedel-Niedrig, T.; Weiss, W.; Schlögl, R. Electronic Structure of Ultrathin Ordered Iron Oxide Films Grown onto Pt(111). *Phys. Rev. B* **1995**, *52*, 17449–17460.
34. Kim, Y. J.; Westphal, C.; Ynzunza, R. X.; Wang, Z.; Galloway, H. C.; Salmeron, M.; Van Hove, M. A.; Fadley, C. S. The Growth of Iron Oxide Films on Pt(111): A Combined XPD, STM, and LEED Study. *Surf. Sci.* **1998**, *416*, 68–111.
35. Ritter, M.; Ranke, W.; Weiss, W. Growth and Structure of Ultrathin FeO Films on Pt(111) Studied by STM and LEED. *Phys. Rev. B* **1998**, *57*, 7240–7251.
36. Ranke, W.; Ritter, M.; Weiss, W. Crystal Structures and Growth Mechanism for Ultrathin Films of Ionic Compound Materials: FeO(111) on Pt(111). *Phys. Rev. B* **1999**, *60*, 1527–1530.
37. Merte, L. R.; Knudsen, J.; Grabow, L. C.; Vang, R. T.; Lægsgaard, E.; Mavrikakis, M.; Besenbacher, F. Correlating STM Contrast and Atomic-Scale Structure by Chemical Modification: Vacancy Dislocation Loops on FeO/Pt(111). *Surf. Sci.* **2009**, *603*, L15–L18.
38. Knudsen, J.; Merte, L. R.; Grabow, L. C.; Eichhorn, F. M.; Porsgaard, S.; Zeuthen, H.; Vang, R. T.; Lægsgaard, E.; Mavrikakis, M.; Besenbacher, F. Reduction of FeO/Pt(111) Thin Films by Exposure to Atomic Hydrogen. *Surf. Sci.* **2010**, *604*, 11–20.
39. Zeuthen, H.; Kudernatsch, W.; Peng, G. W.; Merte, L. R.; Ono, L. K.; Lammich, L.; Bai, Y. H.; Grabow, L. C.; Mavrikakis, M.; Wendt, S.; Besenbacher, F. Structure of Stoichiometric and Oxygen-Rich Ultrathin FeO(111) Films Grown on Pd(111). *J. Phys. Chem. C* **2013**, *117*, 15155–15163.
40. Merte, L. R.; Grabow, L. C.; Peng, G.; Knudsen, J.; Zeuthen, H.; Kudernatsch, W.; Porsgaard, S.; Lægsgaard, E.; Mavrikakis, M.; Besenbacher, F. Tip-Dependent Scanning Tunneling Microscopy Imaging of Ultrathin FeO Films on Pt(111). *J. Phys. Chem. C* **2011**, *115*, 2089–2099.
41. Zeuthen, H. *Atomic Scale Investigation of Ultra-Thin Iron Oxides Supported on Pt(111) and Pd(111)*. Ph.D. Thesis, Aarhus University, 2012.
42. Predel, B. Fe-Pt (Iron-Platinum). In *Landolt-Börnstein - Group IV Physical Chemistry numerical Data and Functional Relationships in Science and Technology*; Madelung, O., Ed.; Springer Verlag: Berlin/Heidelberg, 1995; 10.1007/10474837_10471330.
43. Giordano, L.; Lewandowski, M.; Groot, I. M. N.; Sun, Y. N.; Goniakowski, J.; Noguera, C.; Shaikhutdinov, S.; Pacchioni, G.; Freund, H. J. Oxygen-Induced Transformations of an FeO(111) Film on Pt(111): A Combined DFT and STM Study. *J. Phys. Chem. C* **2010**, *114*, 21504–21509.
44. Giordano, L.; Pacchioni, G.; Goniakowski, J.; Nilius, N.; Rienks, E. D. L.; Freund, H. J. Interplay between Structural, Magnetic, and Electronic Properties in a FeO/Pt(111) Ultrathin Film. *Phys. Rev. B* **2007**, *76*, 075416.
45. Lægsgaard, E.; Besenbacher, F.; Mortensen, K.; Stensgaard, I.; Fully, A. Automated, Thimble-Size Scanning Tunnelling Microscope. *J. Microsc.* **1988**, *152*, 663–669.
46. Lauritsen, J. V.; Besenbacher, F. Model Catalyst Surfaces Investigated by Scanning Tunneling Microscopy. *Adv. Catal.* **2006**, *50*, 97–147.